Influence of radiation damage on diffusion of fission products in silicon carbide

E. Friedland*, T.T. Hlatshwayo, N.G. van der Berg

Physics Department, University of Pretoria, Pretoria, South Africa

*Corresponding author. E mail: erich.friedland@up.ac.za, Phone: +27-12-4202453, Fax: +27-12-3625288

The influence of irradiation induced damage on the transport of implanted species in poly and single crystalline silicon carbide is investigated. For this purpose published diffusion results of strontium, silver, iodine and cesium are compared with the associated evolution of defect profiles determined by α-particle channelling in a backscattering geometry. Strong diffusion takes place in the amorphized surface layer of room temperature implanted 6H-SiC during annealing at 1100 °C, which drops below the detection limit of 10^{-21} m^2 s^{-1} as soon as re-crystallization is completed. Diffusion in samples implanted above the critical amorphization temperature is only observed when simultaneously a significant reduction of defect density occurs. No diffusion into the undamaged bulk is detected at temperatures up to 1500 °C. The observed diffusion behaviour is explained by a defect related trapping and release mechanism. Normal grain boundary diffusion of silver and iodine occurs in CVD-SiC.

Keywords silicon carbide, diffusion, radiation damage

1 Introduction Fuel particles of modern high-temperature nuclear reactors (HTR's) are encapsulated by CVD-layers which serve as barriers to prevent fission product release. Recent reactor designs generally make use of fuel kernels surrounded by four successive layers of low-density pyrolitic carbon, high-density pyrolitic carbon, silicon carbide and high-density pyrolitic carbon, with silicon carbide being the main barrier for the metallic species. These so-called TRISO fuel particles retain quite effectively most of the important fission products up to temperatures of 1000 °C [1]. Currently design studies are considered for the *International Generation IV Reactor Program*, operating at temperatures significantly above 1000 °C to enhance their efficiency, especially in view of process heat applications for hydrogen generation [2]. However, little reliable information on transport properties of fission products in silicon carbide above this temperature is available.

Radio-active isotopes of strontium, iodine and cesium are important fission products of radio-ecological relevance because of their possible accumulation in the human body. Strontium is due to its chemical similarity to calcium easily deposited in bones, while iodine is accumulated in the thyroid gland and cesium in muscular tissue with biological half-lives of approximately 140 days. The stable silver isotope ^{109}Ag, on the other hand, can present serious maintenance problems in modern HTR's because of its probability to produce the highly radio-active isotope ^{110}Ag by neutron capture. Due to the relatively high vapour pressure of silver at the envisaged operating temperature it might contaminate the cooling gas and consequently all equipment like pumps and heat exchangers in the primary cooling circuit.

Diffusion investigations of the above mentioned four elements in silicon carbide at temperatures above 1000 °C were recently reported by our group [3-8]. To understand their diffusion behaviour, these results are compared with the accompanying evolution of the irradiation induced damage during ion implantation.

2 Experiment and analysis Hexagonal 6H-SiC from *Intrinsic Semiconductors*® and CVD-SiC from *Valley Design Corporation*®, having a columnar structure of mainly 3C-SiC crystallites, were used in the investigations. The relevant ions were implanted at room temperature (RT), 350 °C and 600 °C into the wafers with energy of 360 keV and a flux not exceeding 10^{13} cm^{-2} s^{-1}. Fluences of 2×10^{16} cm^{-2} for strontium and silver and 1×10^{16} cm^{-2} for iodine and cesium were implanted to obtain maximum concentrations of about 1%. The different implantation temperatures made it possible to compare transport processes in amorphous, poly and single crystalline silicon carbide. Diffusion was determined from the broadening of the implantation profiles after isochronal and isothermal annealing studies using RBS analysis. In the case of single crystalline samples these measurements were combined with the results of α-particle channelling spectroscopy to obtain defect density profiles as a function of implantation and annealing temperatures. Structural information on the samples before and after annealing was obtained by scanning electron microscopy (SEM). A detailed description of the experimental techniques is given elsewhere [5].

Diffusion coefficients were extracted from the broadening of implantation profiles during isothermal annealing. If they can be described by a Gaussian depth distribution the following relationship between the final and original widths holds [9].

$$[W(t)]^2 = 4Dt\ \ln(2) + [W(0)]^2,$$

where $W(t)$ is defined as the full width at half-maximum after annealing for time t. Hence, the diffusion coefficient D is directly obtained from the slope of a plot of $[W(t)]^2$ versus annealing time t at constant temperature.

Damage profiles where obtained from the channelling spectra along the (0001) direction using the computer code DICADA [10]. This code makes use of a modified master equation approach based on the channelling concept of the Lindhard theory. The latter theory under-estimates the yield of the aligned spectrum because of the assumption that conservation of transverse energy in an ideal crystal holds right from the surface, while this is only true after the ions have penetrated a relatively large number of atomic layers. This is rectified in the modified master equation by using start values for the minimum yield at the surface obtained from a full simulation. DICADA calculations can be applied to compounds containing different kinds of point defect configurations, including clusters and amorphous zones. However, it does not take into account stacking faults and dislocation loops, which have relatively large de-channelling cross sections. When these extended defects are present, artificial tail-effects at larger depths are obtained. Assuming randomly displaced atoms, we observed this effect in all samples. For our calculations we used a Debye temperature of $\Theta_D = 1030\ K$, which is an average of the widely varying published values [11]. Furthermore lattice parameters of $a = 0.3081$ nm, $c = 1.5092$ nm and an atomic density of $\rho = 9.641\times10^{22}\ at\ cm^{-3}$ were assumed.

3 Results and discussion In this chapter our previous results [3-8] are compared with the evolution of defect profiles during isothermal and isochronal annealing calculated from channeling spectra employing the DICADA code.

3.1 Strontium implants

Strontium diffusion in SiC was previously investigated by us in cold and hot implanted single and poly crystalline wafers [6]. In Fig. 1 random and aligned spectra are shown of samples implanted at RT, 350 °C and 600 °C. While the surface region is completely disordered in the room temperature implant, the basic crystal structure is retained in both hot implants, albeit with varying

damage densities. A similar temperature dependence of damage profiles is obtained with many others ion species [12], including those of this investigation. Selected spectra of the RT-implant during isochronal annealing, starting at 900 °C with an increase of 100 °C between each 5 hour cycle, are depicted in Fig. 2 together with the corresponding SEM-images. The as-implanted surface is, except of some polishing lines, absolutely featureless, which is typical for a highly disordered or amorphous surface layer. From the aligned spectrum a thickness of 240 nm for this surface region is deducted. During annealing epitaxial regrowth from the bulk and re-crystallization compete with each other, eventually resulting in a relatively stable poly-crystalline surface layer of about 180 nm thickness. Hence, the implanted strontium is initially almost entirely embedded in amorphous and later in poly-crystalline silicon carbide. From the SEM-images it is obvious, that already after the 1000 °C annealing cycle a poly-crystalline structure has formed at the surface. Strong diffusion towards the surface and none into the undamaged bulk can be concluded from the shape of the strontium peak. At temperatures of 1200 °C and higher, significant loss of strontium through the surface occurs during isochronal annealing.

The diffusion behaviour during isothermal annealing is plotted in Fig. 3. Strong diffusion is observed during the first 5 hours in single and poly-crystalline samples implanted at RT, but no further diffusion occurs during prolonged isothermal annealing. In samples implanted at 600 °C a much smaller width broadening occurs during the first annealing cycle, but otherwise they exhibit the same behaviour during further annealing. Hence, the diffusion coefficients after the initial heating cycle in poly and single crystalline samples are below our detection limit of approximately 10^{-21} m^2 s^{-1} at temperatures up to 1400 °C. Fig 4 shows the damage evolution during isothermal annealing at 1200 °C and 1300 °C together with the corresponding diffusion and retention results. At both temperatures strong damage reduction occurs during the first annealing step, while further annealing does not change the defect densities significantly. Although at the higher temperature a considerably lower defect density is obtained, this does not result in markedly different diffusion during the first annealing step. Very little strontium, if any, is lost from the surface during the first annealing cycle, while no further loss is observable during prolonged isothermal annealing at either temperature

3.2 Silver implants

Similarly as discussed above, RT implantations of silver ions at a fluence of 2×10^{16} cm^{-2} lead to an amorphous surface region, while the crystalline structure is retained if implanted above 350 °C [3]. Preliminary annealing of the RT-implant for 2 hours at 960 ºC caused an epitaxial re-growth from the bulk to reduce the amorphous surface region from 260 nm to about 220 nm of poly-crystalline matter. Complete transformation of the entire amorphous layer during annealing to a poly-crystalline phase is confirmed by Raman spectroscopy [8]. For all practical purposes the implanted silver profile with a projected range of R_p = 106 nm is now embedded in the re-crystallized surface region and its depth profile had not changed significantly.

Fig. 5 displays the evolution of damage profiles of 6H-SiC samples implanted at RT and 350 °C during isothermal annealing at 1300 °C together with the corresponding annealing curves, including one of a CVD-SiC sample implanted at 350 °C. Similarly as found previously for strontium implants, a strong reduction of the defect densities occur during the first annealing cycle, while no further change is observable during additional annealing cycles. A relatively large depth broadening is found after the first 10 hours of annealing for the RT implanted 6H-SiC, but subsequent heat treatments do not change the width of the silver depth profile any further. In agreement with the results of ref. [13] no depth broadening at all is observed for 6H-SiC implanted at 350 °C indicating again a diffusion coefficient of less than 10^{-21} m^2 s^{-1}. The annealing curve of the CVD-SiC sample exhibits a linear increase from which a diffusion coefficient of about 3×10^{-20} m^2 s^{-1} can be

extracted. Grain boundary diffusion must be responsible for the silver transport, as no volume diffusion was detected in the hot implanted 6H-SiC. This observation is in stark contrast to the result obtained for the RT-implant of 6H-SiC, which has also transformed to a poly-crystalline structure during annealing. In the latter case, however, diffusion is only observed during the first annealing stage, when the surface layer is still amorphous.

3.3 Iodine implants

Iodine diffusion in single and polycrystalline silicon carbide was previously investigated in samples implanted at RT, at 350 °C and at 600 °C [6]. The iodine transport observed in the cold implants displays an abnormally large increase at 1200 °C, which is difficult to explain by Fickian diffusion. Severe topographical changes of the surface, with no corresponding large iodine losses are observed. This phenomenon points to a reaction, binding iodine to the amorphized silicon carbide during high-temperature annealing. In contrast to this, normal conditions seem to prevail in the hot implants, which leave the samples in the somewhat lower energy state of crystalline matter. Fig. 6 shows the evolution of damage profiles in the 600 °C implants during isothermal annealing at 1200 °C and 1300 °C together with the corresponding annealing curves for single and polycrystalline samples. The results for iodine differ in two ways from those of the other three implants. Both the damage reduction and diffusion is not completed during the first annealing stage but only at some later time. Secondly the de-channeled fraction in the tail region is about twice as large as observed for the other implants. This indicates a significantly higher density of extended defects, which might be related to the same phenomenon observed during the cold iodine implant. Iodine diffusion is observed in all samples at the early stages of isothermal annealing, while after a certain time it stops or is considerably reduced. At 1200 °C no diffusion is detected after the initial two stages in either 6H-SiC or CVD-SiC. Although the reduction of defect density is significantly larger at 1300 °C, the final broadening of the profile widths of the 6H-SiC samples is found to be similar at both temperatures within experimental error. The diffusion coefficient of 6H-SiC is at both temperatures below our detection limit of 10^{-21} m^2 s^{-1}. The same is true for CVD-SiC at 1200 °C, for which after prolonged heating no further profile width broadening is observed, However, at 1300 °C the width increases linearly with annealing time, which indicates again grain boundary diffusion with an effective diffusion coefficient of about 7×10^{-21} m^2 s^{-1}.

3.4 Cesium implants

Diffusion properties of cesium in single and polycrystalline SiC are discussed in ref. [7]. The evolution of damage profiles during isothermal annealing at 1200 °C, 1300 °C and 1400 °C of samples implanted at 600 °C is shown in Fig. 7. During the first annealing cycle a large reduction of defect density occurs in all three cases with no further reduction during subsequent cycles. Neither during the initial cycle nor during prolonged annealing any width broadening within experimental error can be detected, although defect reduction at the two higher temperatures is significantly larger than at 1200 °C. Fig. 8 depicts the isochronal annealing results for 6H-SiC implanted at 600 °C, together with an annealing curve for RT implantation. The high-temperature implant shows no width broadening up to 1200 °C. However, above this temperature a continuous increase of the width occurs, which seems to contradict the isothermal behaviour discussed above. Simultaneously a significant reduction of defect densities is observed during each annealing step, starting with the first cycle at 1100 °C. The RT implant shows the usual initial depth broadening due to cesium diffusion in the amorphized surface region and furthermore a similar behaviour as the high-temperature implant with a somewhat larger diffusion rate above 1200 °C. The cesium loss of about 50% from the samples implanted at RT and 350 °C occurs only during the initial annealing cycles when amorphous material is still available.

4 Conclusion The large profile broadening after the first annealing period of RT implants into 6H-SiC is certainly due to enhanced diffusion in the amorphous surface region caused by ion irradiation. Initially the implantation profiles are completely embedded in amorphous silicon carbide, which changes relatively fast into a finely grained poly-crystalline layer during annealing at 1000 °C. Although it has a somewhat reduced thickness because of epitaxial re-growth, most of the implanted atoms are still surrounded by it. One would expect that the large amount of grain boundaries in this layer provides a multitude of diffusion paths, along which the implanted species diffuse towards the surface during further annealing. This, however, is not the case. In all cases investigated the diffusion stops after some time, indicating that it only takes place in the amorphous and not in the re-crystallized material. This is confirmed by the observation that only during the first cycle any impurity loss occurs, which is especially puzzling for silver implants, where relatively strong grain boundary diffusion is observed in CVD-SiC after hot implantation. A possible reason for this might be the different grain boundary structure of CVD-SiC and the re-crystallized zone of 6H-SiC. Another possible explanation is the presence of diffusion enhancing impurities in the grain boundaries of CVD-SiC, which are not expected in the re-crystallized zone of high-purity 6H-SiC.

Hot implanted 6H-SiC samples retain the basic single crystal structure, although with a relatively high defect density. At annealing temperatures up to 1100 °C diffusion of the implanted species is below our detection limit. Above this temperature diffusion occurs in some cases during the initial isothermal annealing cycle in the radiation damaged zone but stops afterwards. However, independent of this, strong reduction of defect densities during the initial heating cycles is observed in all cases, with very little change during further prolonged heating at constant temperature. Furthermore, only forward diffusion is observed in 6H-SiC up to temperatures of 1400 °C, while no diffusion into the undamaged bulk is found. Only in CVD-SiC silver and iodine transport takes place in both directions, indicating a normal grain boundary diffusion process. However, in contrast to the isothermal annealing results, a constantly increasing diffusion rate, starting above 1200 °C, is observed during isochronal annealing of cesium implants. Simultaneously a significant reduction of the defect density occurs during each annealing cycle from 1100°C up to 1500 °C.

It is noteworthy that impurity diffusion in 6H-SiC is only observed when simultaneously the defect density is significantly reduced, although the opposite is not necessarily true. This observation points to a trapping and release mechanism of impurities by defect structures. In all cases investigated in this study, diffusion processes occur only during periods of defect annealing and stop as soon as defect restructuring is coming to an end. Impurity atoms bound to defect complexes are released during their annihilation or restructuring and then diffuse in the distorted lattice structure, until being captured again after some time by more stable defects. During isochronal annealing this can happen after each cycle at an increased temperature, while it can only occur during the first cycle during isothermal annealing. No diffusion is observed in the undistorted lattice beyond the irradiation zone at temperatures employed in this investigation.

Acknowledgements Financial support of the *National Research Foundation* and the *Bundesministerium für Bildung und Forschung* is gratefully acknowledged.

References

[1] D. Hanson, A Review of Radionuclide Release from HTGR Cores During Normal Operation, Electric Power Research Institute, Report 1009382, March 2004.

[2] National Hydrogen Energy Roadmap, United States Department of Energy, Washington, DC, November 2002.

[3] E. Friedland, J.B. Malherbe, N.G. van der Berg, T Hlatshwayo, A.J Botha, E. Wendler, W. Wesch, J. Nucl. Mater. 389, 326 (2009).

[4] E. Friedland, N.G. van der Berg, J.B. Malherbe, R.J. Kuhudzai, A.J. Botha, E. Wendler, W. Wesch, Nucl. Instr.. and Meth. B 268, 2892 (2010).

[5] E. Friedland, N.G. van der Berg, J.B. Malherbe, J.J. Hanke, J. Barry, E. Wendler, W. Wesch, J. Nucl. Mater. 410, 24 (2011).

[6] E. Friedland, N.G. van der Berg, J.B. Malherbe, E. Wendler,. W. Wesch, J. Nucl. Mater. 425, 205 (2012).

[7] E. Friedland, N.G. van der Berg, T.T. Hlatshwayo, R.J. Kuhudzai, J.B. Malherbe, E. Wendler, W. Wesch, Nucl. Instr. and Meth. B 286 102 (2012).

[8] T.T. Hlatshwayo, J.B. Malherbe, N.G. van der Berg, L.C. Prinsloo, A.J. Botha, E. Wendler, W. Wesch, Nucl. Instr. and Meth. B 274 120 (2012).

[9] S.M. Myers, S.T. Picraux, T.S. Prevender, Phys. Rev. B 9, 3953 (1974).

[10] K. Gärtner, Nucl. Instr. and Meth. B 227, 522 (2005).

[11] L.L.Snead, T.Nozawa, Y. Katoh, T.-S. Byun, S. Kondo, D.A. Petty, J. Nucl. Mater. 371, 329 (2007).

[12] E. Wendler, A. Heft, W. Wesch, Nucl. Instr. and Meth. B 141, 105 (1998).

[13] W. Jiang, W.J. Weber, V. Shutthanandan, L. Li, S. Thevuthasan, Nucl. Instr. and Meth. B 219/220, 642 (2004).

Figure captions

Fig. 1: Random and aligned spectra of 6H-SiC as-implanted at RT, 350 °C and 600 °C with a fluence of 2×1016 Sr+ cm-2 at 360 keV taken from reference [6].

Fig. 2: Spectra of the strontium implant at RT before and after isochronal annealing at 1000 °C and 1200 °C together with the corresponding SEM-images including magnification bars.

Fig. 3: Isothermal annealing curves at different temperatures for single and poly-crystalline samples implanted with strontium at RT and 600 °C taken from reference [6]. Lines are drawn to guide the eye.

Fig. 4: Evolution of damage profiles of samples implanted with strontium at 600 °C during isothermal annealing at 1200 °C and 1300 °C. Also shown are the corresponding annealing and retention curves. Lines are drawn to guide the eye.

Fig. 5: Evolution of damage profiles of samples implanted with silver at RT and 350 °C during isothermal annealing at 1300 °C. Also shown are corresponding annealing curves and one of a polycrystalline sample implanted at 350 °C. Lines are drawn to guide the eye.

Fig. 6: Evolution of damage profiles of samples implanted with iodine at 600 °C during isothermal annealing at 1200 °C and 1300 °C. Also shown are corresponding annealing curves for single and polycrystalline samples taken from reference [6]. Lines are drawn to guide the eye.

Fig. 7: Evolution of damage profiles of samples implanted with cesium at 600 °C during isothermal annealing at 1200 °C, 1300 °C and 1400 °C Also shown are the corresponding annealing curves

Fig. 8: Evolution of damage profiles of a 6H-SiC sample implanted with cesium at 600 °C dur-ing isochronal annealing of 5 hour cycles. Also shown is the corresponding annealing curve together with one for RT implantation. Lines are drawn to guide the eye.

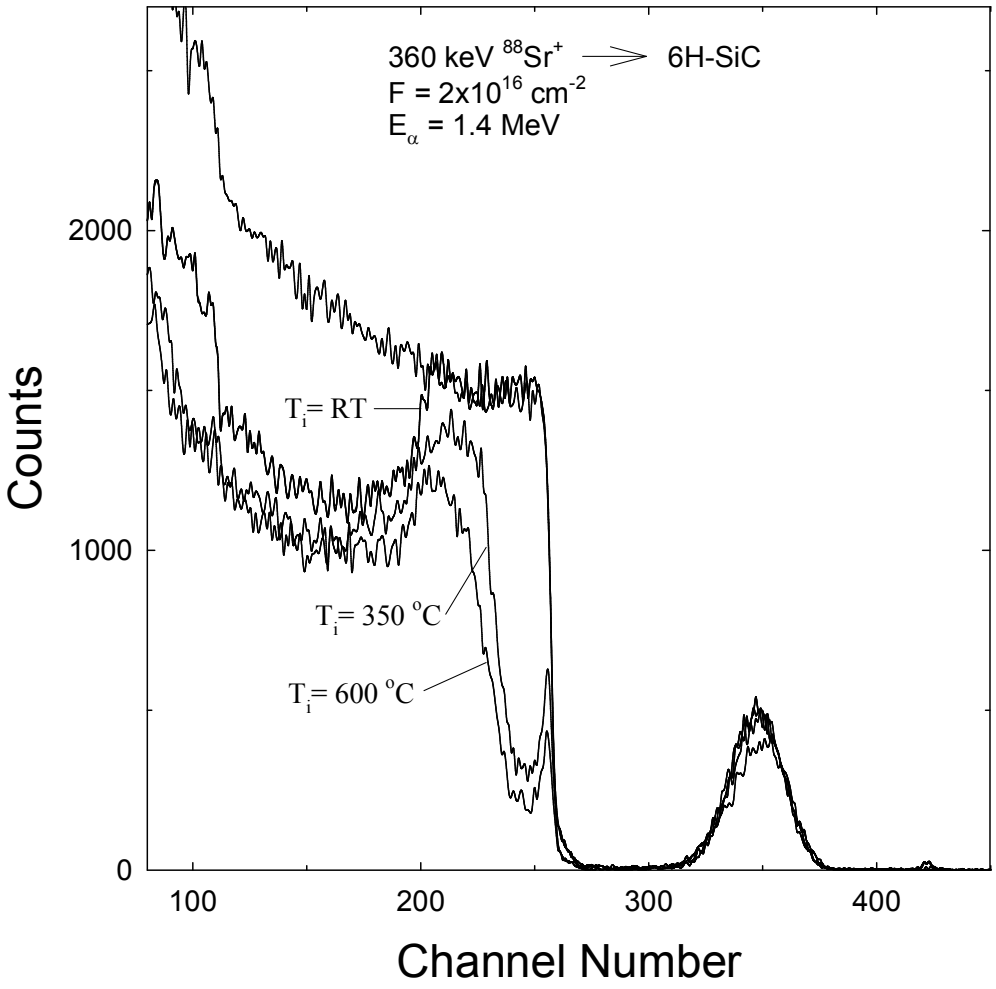
360 keV $^{88}Sr^{+}$ → 6H-SiC
F = 2x10^{16} cm^{-2}
E_α = 1.4 MeV
T_i= RT
T_i= 350 °C
T_i= 600 °C
Counts
Channel Number
0
1000
2000
100
200
300
400

Figure 1

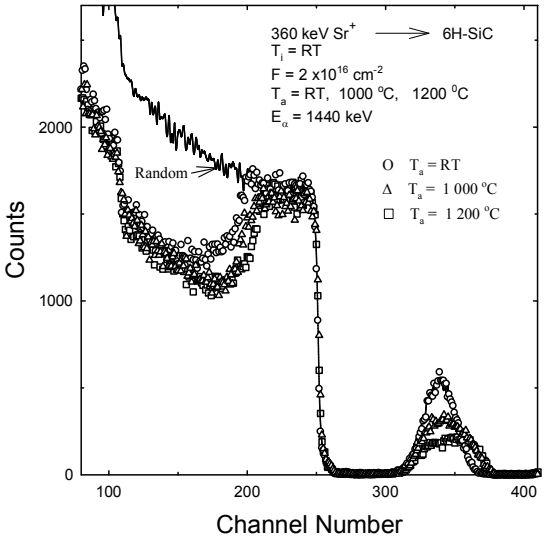

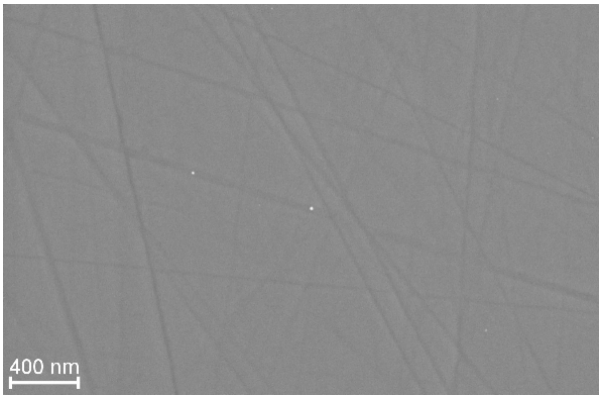

As-implanted

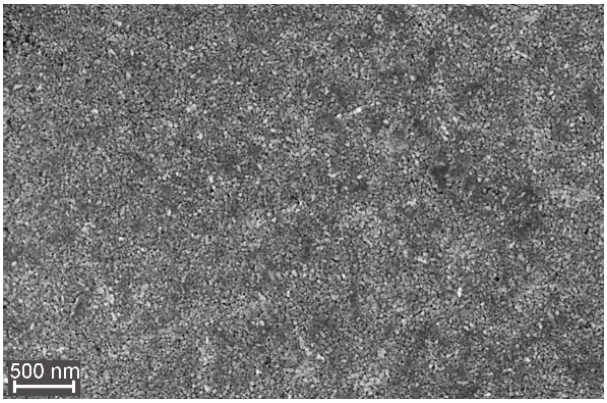

T_a = 1000 °C; t_a = 5 h

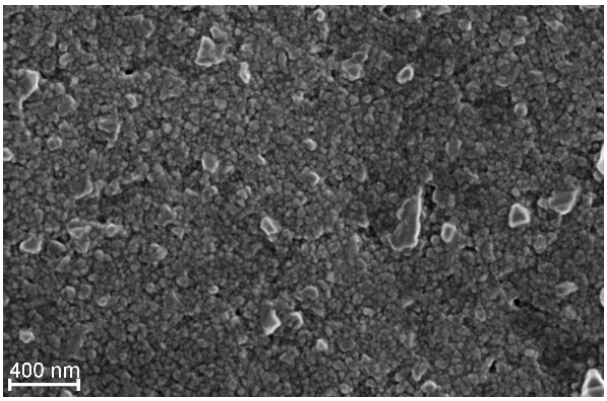

T_a = 1200 °C; t_a = 5 h

Figure 2

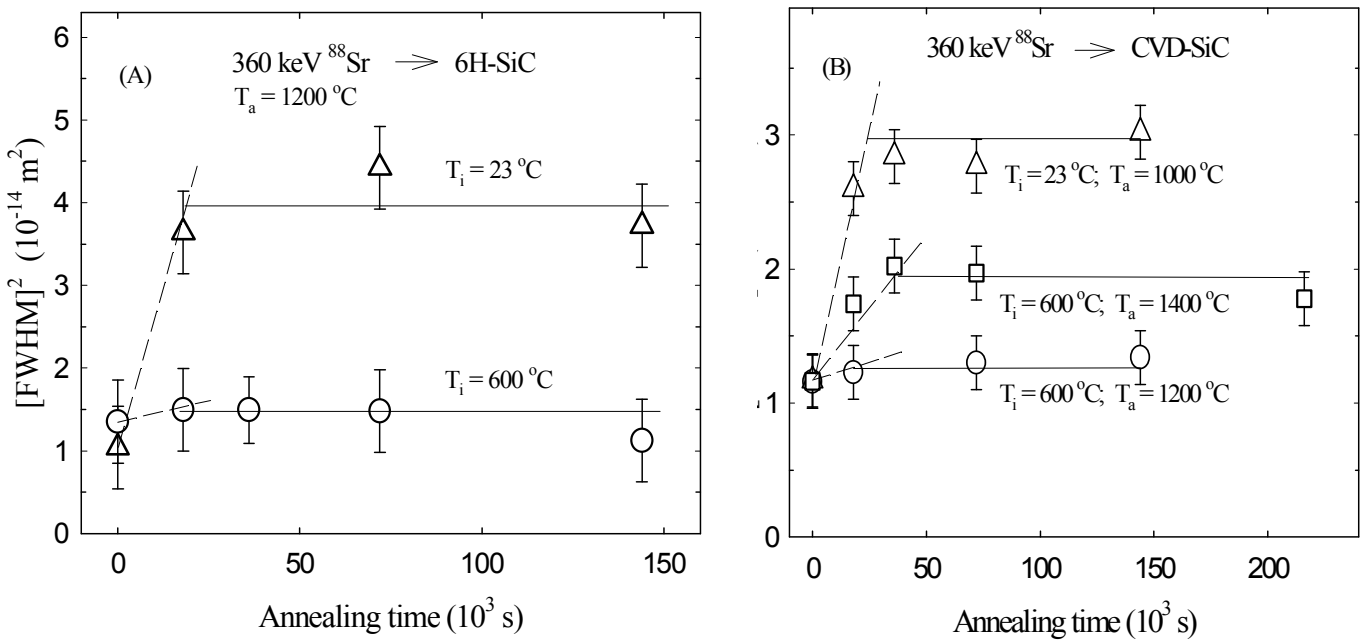
(A)
360 keV ^{88}Sr → 6H-SiC
T_a = 1200 °C
T_i = 23 °C
T_i = 600 °C
[FWHM]^2 (10^{-14} m^2)
Annealing time (10^3 s)
(B)
360 keV ^{88}Sr → CVD-SiC
T_i = 23 °C; T_a = 1000 °C
T_i = 600 °C; T_a = 1400 °C
T_i = 600 °C; T_a = 1200 °C
Annealing time (10^3 s)

Figure 3

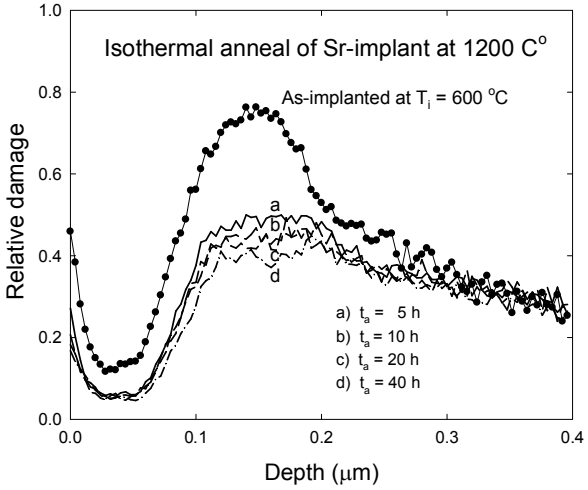
Isothermal anneal of Sr-implant at 1200 C°
As-implanted at T_i = 600 °C
a
b
c
d
a) t_a = 5 h
b) t_a = 10 h
c) t_a = 20 h
d) t_a = 40 h
Relative damage
Depth (μm)

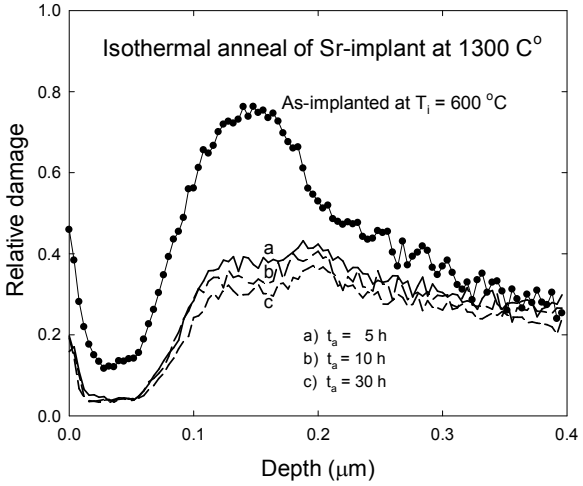
Isothermal anneal of Sr-implant at 1300 C°
As-implanted at T_i = 600 °C
a
b
c
a) t_a = 5 h
b) t_a = 10 h
c) t_a = 30 h
Relative damage
Depth (μm)

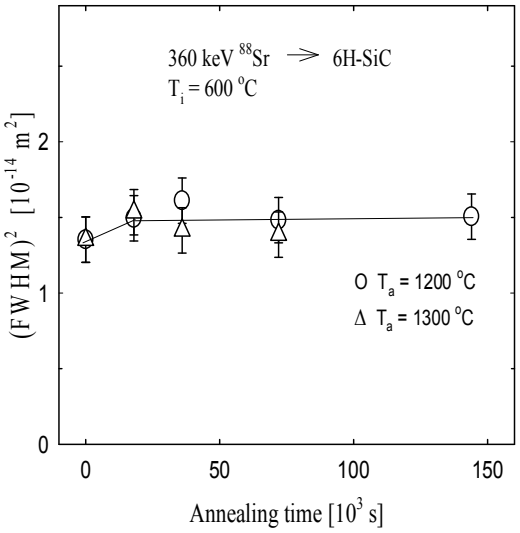
360 keV 88Sr → 6H-SiC
T_i = 600 °C
O T_a = 1200 °C
Δ T_a = 1300 °C
(FWHM)² [10⁻¹⁴ m²]
Annealing time [10³ s]

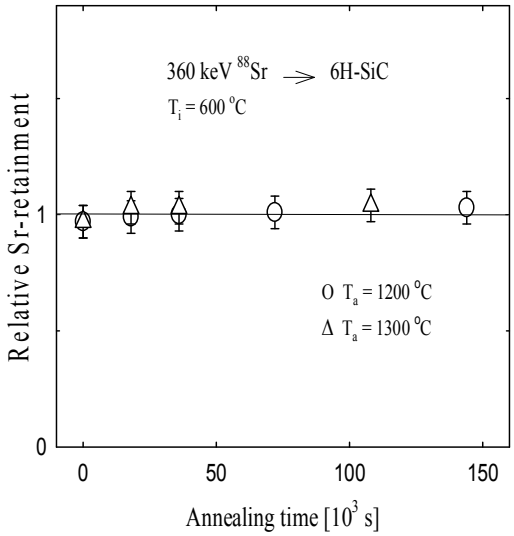
360 keV 88Sr → 6H-SiC
T_i = 600 °C
O T_a = 1200 °C
Δ T_a = 1300 °C
Relative Sr-retainment
Annealing time [10³ s]

Figure 4

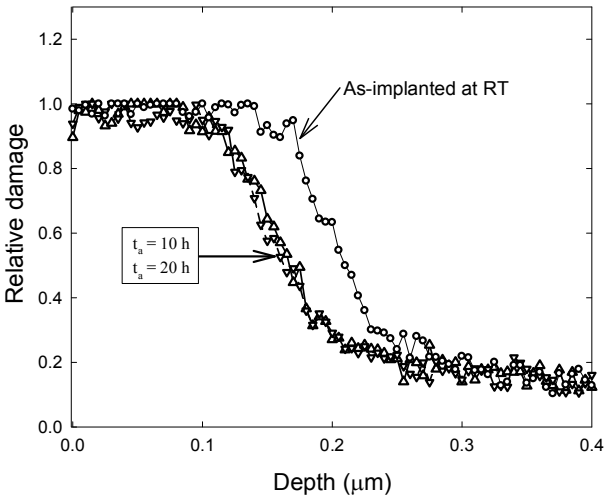
As-implanted at RT
t_a = 10 h
t_a = 20 h
Relative damage
Depth (μm)

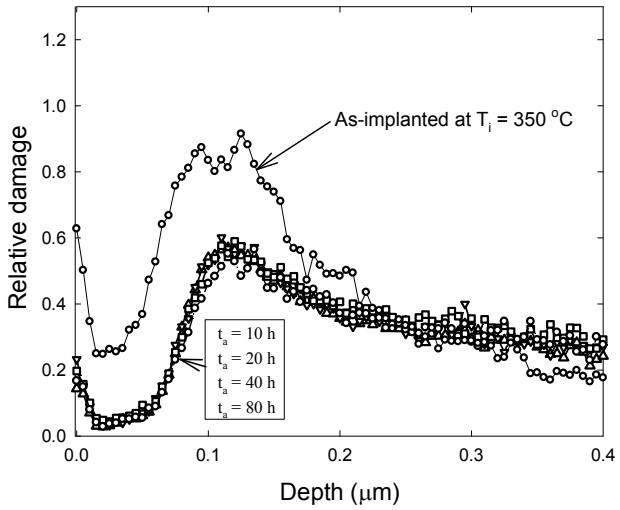
As-implanted at T_i = 350 °C
t_a = 10 h
t_a = 20 h
t_a = 40 h
t_a = 80 h
Relative damage
Depth (μm)

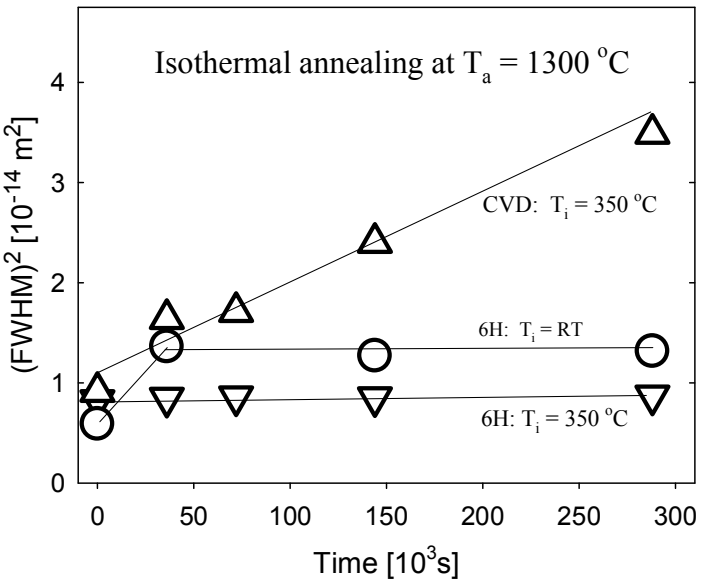
Isothermal annealing at T_a = 1300 °C
CVD: T_i = 350 °C
6H: T_i = RT
6H: T_i = 350 °C
$(FWHM)^2$ [10^{-14} m^2]
Time [10^3s]

Figure 5

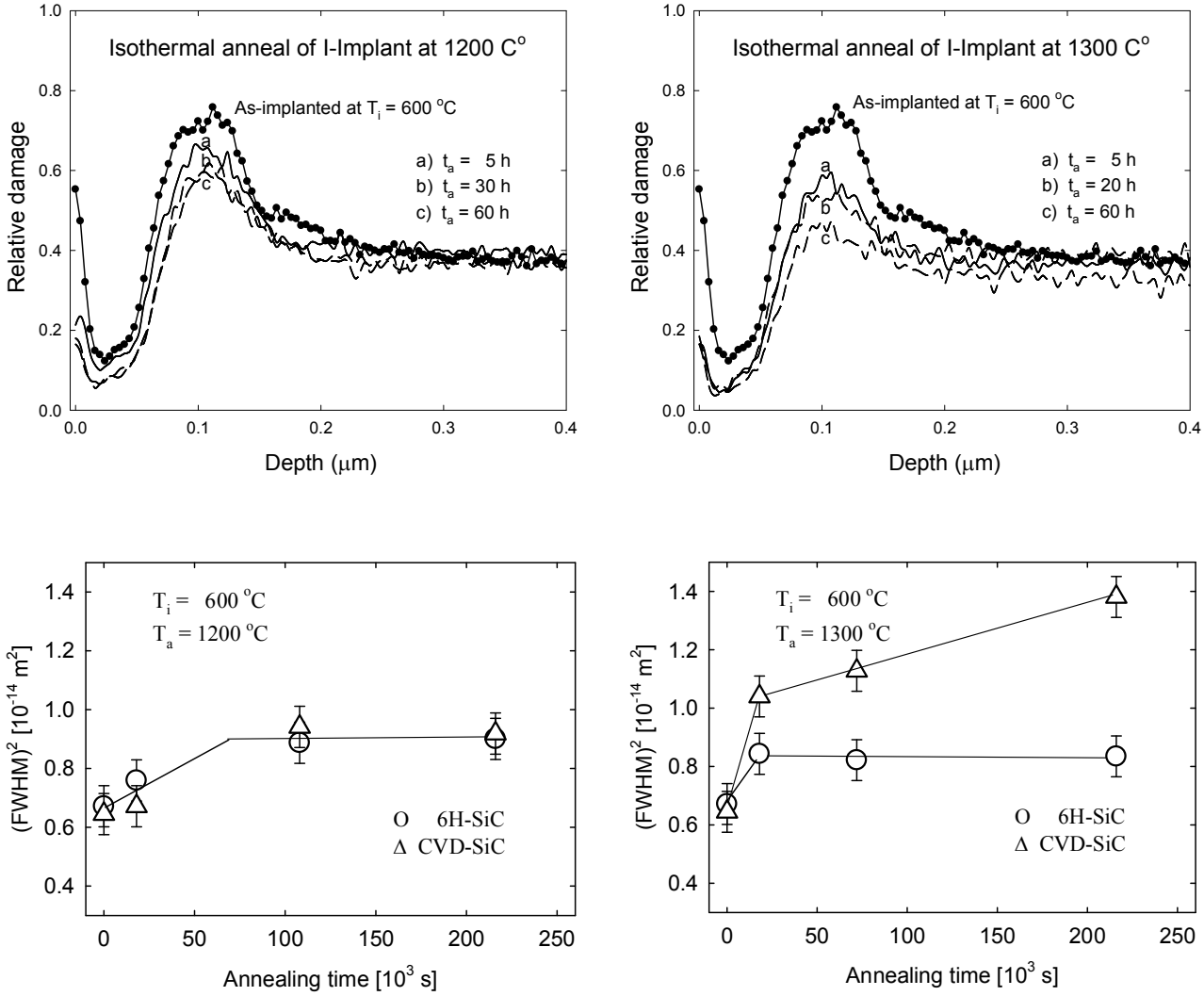
Isothermal anneal of I-Implant at 1200 C°
As-implanted at T_i = 600 °C
a) t_a = 5 h
b) t_a = 30 h
c) t_a = 60 h
Relative damage
Depth (μm)
Isothermal anneal of I-Implant at 1300 C°
As-implanted at T_i = 600 °C
a) t_a = 5 h
b) t_a = 20 h
c) t_a = 60 h
Relative damage
Depth (μm)
T_i = 600 °C
T_a = 1200 °C
O 6H-SiC
Δ CVD-SiC
(FWHM)² [10⁻¹⁴ m²]
Annealing time [10³ s]
T_i = 600 °C
T_a = 1300 °C
O 6H-SiC
Δ CVD-SiC
(FWHM)² [10⁻¹⁴ m²]
Annealing time [10³ s]

Figure 6

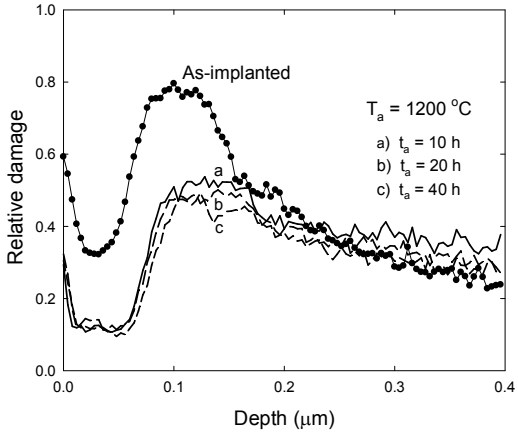
As-implanted
T_a = 1200 °C
a) t_a = 10 h
b) t_a = 20 h
c) t_a = 40 h
Relative damage
Depth (μm)

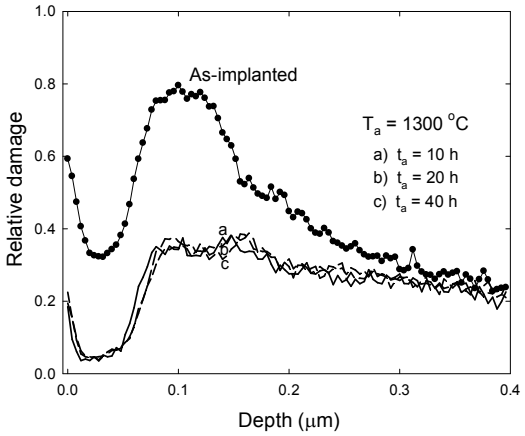
As-implanted
T_a = 1300 °C
a) t_a = 10 h
b) t_a = 20 h
c) t_a = 40 h
Relative damage
Depth (μm)

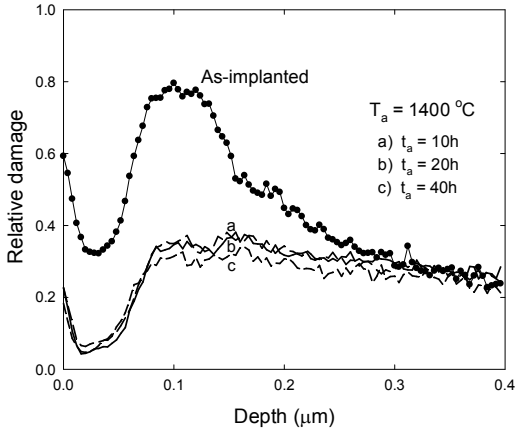
As-implanted
T_a = 1400 °C
a) t_a = 10h
b) t_a = 20h
c) t_a = 40h
Relative damage
Depth (μm)

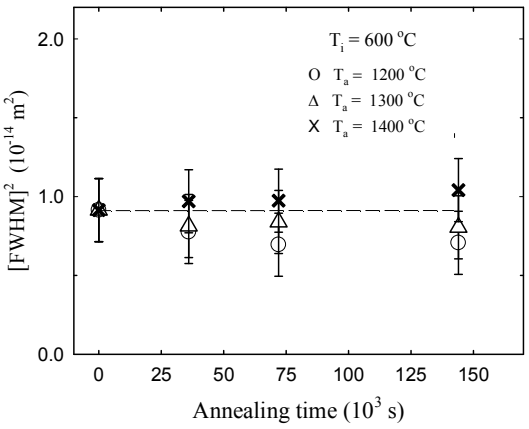
T_i = 600 °C
O T_a = 1200 °C
Δ T_a = 1300 °C
X T_a = 1400 °C
$[FWHM]^2$ (10^{-14} m^2)
Annealing time (10^3 s)

Figure 7

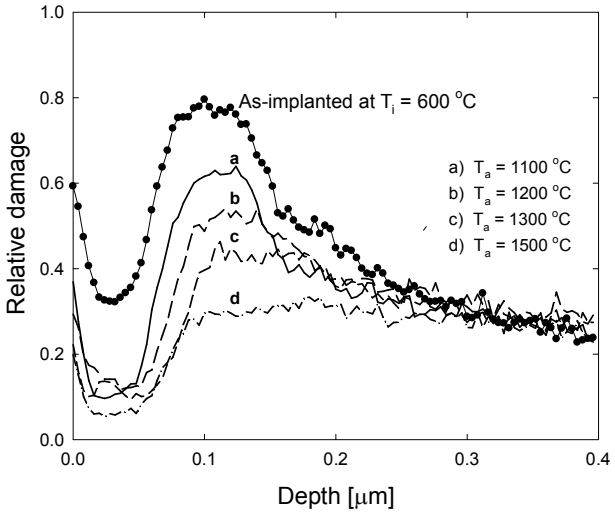
Relative damage
Depth [μm]
As-implanted at T_i = 600 °C
a) T_a = 1100 °C
b) T_a = 1200 °C
c) T_a = 1300 °C
d) T_a = 1500 °C
a
b
c
d

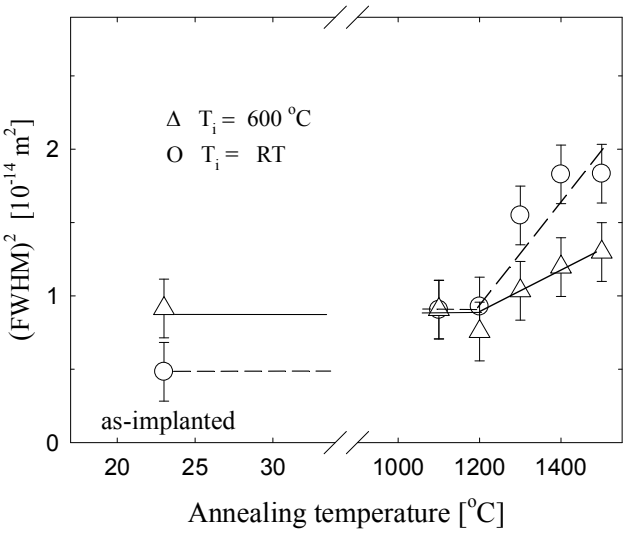
$(FWHM)^2$ [10^{-14} m^2]
Δ T_i = 600 °C
O T_i = RT
as-implanted
Annealing temperature [°C]

Figure 8